Local and long-range realizations of a spin-reorientation surface phase transition

G. He, H. Winch, R. Belanger, P. H. Nguyen, and D. Venus[*]

Department of Physics and Astronomy, McMaster University, Hamilton, Ontario, Canada

(Received 25 October 2016; revised manuscript received 20 January 2017; published 8 March 2017)

The spin-reorientation transition of an ultrathin film from perpendicular to in-plane magnetization is driven by a competition between dipole and anisotropy energies. *In situ* measurements of the magnetic susceptibility of Fe/2 monolayers (ML) Ni/W(110) films as a function of Fe coverage, made as the films are deposited at constant temperature, show two clear peaks that are described quantitatively as a long-range and a local realization of the transition. In the long-range realization, the susceptibility probes the striped domain pattern that is formed in response to the balance of energetics on a mesoscopic scale. Here the reorientation transition occurs at a noninteger layer thickness. In the local realization, the susceptibility probes the response of small islands with in-plane anisotropy in the third atomic Fe layer that are grown on the second atomic Fe layer, which has perpendicular anisotropy. It is a response to the local finite-size, metastable energetics due to discrete steps in thickness. An excellent quantitative description of the susceptibility data is obtained when both local and long-range aspects of the spin-reorientation transition are included.

I. INTRODUCTION

The spin-reorientation transition observed in ultrathin magnetic films is in reality a complex series of phenomena that illustrates the sensitive balance of exchange, dipole, and anisotropy energies in a two-dimensional magnetic system. In simplest terms, the transition represents the canting of a uniform magnetization between orientations perpendicular and parallel to the surface of the ultrathin film [1–4] in response to a change in the balance of surface anisotropy and dipole energies as a function of either thickness or temperature. In a more complete description, the perpendicularly magnetized state forms an ordered "stripe" pattern of domains with a pattern period that depends sensitively on the proximity of the magnetic reorientation [5–7], and therefore presents an outstanding system for the controlled study of domain formation and dynamics [8,9]. Under even more detailed inspection, it has been found that the ordered domain pattern *itself* undergoes a disordering transition through defect formation [10–13] and might be described by a Kosterlitz–Thouless transition. Given this rich behavior, it is not surprising that the spin-reorientation transition continues to provide fundamental insight into two-dimensional magnetism after over two decades of theoretical and experimental study.

One feature that is often not sufficiently recognized is that there are two separate realizations of the spin-reorientation transition in an ultrathin-film system; a long-range realization and a local realization due to finite-size effects and metastability. Many experimental studies probe large scales where long-range dipole interactions average mesoscopically over the system. Thus one sees reports of the continuous variation of the stripe width in the domain pattern as a function of film thickness as the thickness changes continuously by parts of a tenth of a monolayer, even though film thickness is quantized in atomic monolayers (ML) [14–17]. With the advent of highly spatially resolved studies using spin-polarized scanning tunneling microscopy (STM) or low-energy electron microscopy (LEEM), it is possible to probe local metastable energetics, so that the localized effects of thickness quantization become evident. In this case, a local realization of the transition, at a different location in parameter space, is observed [18,19].

This article reports novel measurements of the magnetic susceptibility of ultrathin Fe/2 ML Ni/W(110) films as a function of coverage as the films are deposited. Magnetic susceptibility provides complementary information to microscopy studies, because it is inherently sensitive to the dynamics of the magnetic excitations of the system, regardless of whether they are on local or long-range scales. The present measurements clearly reveal the distinction between the local and long-range realizations of the spin-reorientation transition through the observation of two distinct peaks in the same continuous measurement of the susceptibility on the same sample. The two peaks are described quantitatively by models based on long-range and local processes and energetics and yield in turn quantitative information about the long-range domain wall density and average dynamics and the distribution of localized island sizes, respectively. Taken together, these provide a more comprehensive, consolidated, and detailed account of the series of phenomena that make up the surface spin-reorientation transition.

II. EXPERIMENTAL METHODS

Measurements of the magnetic susceptibility were made *in situ* as an ultrathin film was grown on a W(110) single-crystal substrate in ultrahigh vacuum. The sample holder [20] was equipped with electron-beam heating for flashing to high temperature, radiative heating for temperature control, and a liquid nitrogen reservoir for cooling. The sample could be rotated through polar and azimuthal angles, so that any in-plane crystalline axis could be aligned with an in-plane pair of magnetic-field coils, and with the scattering plane of the laser beam used for the magneto-optic measurements. For all the data reported here, the in-plane measurement axis was the W[1$\bar{1}$0] direction. A second coil attached to the holder generated a field normal to the sample surface.

———————
[*]venus@physics.mcmaster.ca

The substrate cleanliness was confirmed by using low-energy electron diffraction and Auger-electron spectroscopy (AES).

The films were formed by evaporation from a pure wire. Electrons thermally emitted from a hot filament inside the evaporator [21] were accelerated by 1.75 kV and bombarded the tip of the wire. The sublimated or evaporated atoms were collimated by two apertures and formed a beam directed at the substrate crystal. The evaporator was supported in an adjustable tripod, so that the direction of the atomic beam could be finely adjusted and made to coincide with the region of the film probed by the laser used for magneto-optic Kerr effect (MOKE) measurements. AES was used to iteratively adjust the evaporator direction to ensure a uniform film over a region about 9 mm^2 on the substrate.

The second collimating aperture in the evaporator was electrically isolated. Because a certain fraction of the evaporate atoms striking it are ionized, an ion current of order nA could be measured by using an electrometer. Fine adjustments of the wire position were used to keep the monitor current constant and thus ensure a constant deposition rate. The deposition rate was calibrated by a sequence of accumulating depositions, where the film was annealed to 600 K and an W Auger spectrum was measured after each step in deposition. For Fe/W(110) and Ni/W(110), a plot of the W Auger attenuation vs deposition time shows a clear break in slope at 1 ML that was used to calibrate the monitor current [21,22]. In the present case, the calibration constant for Fe evaporation on W(110) was 3.00 ± 0.15 nA min/ML.

The magnetic susceptibility of the film was determined with a MOKE apparatus [23–25] by using a linearly polarized HeNe laser. Details of the optical arrangement, alignment procedures, sensitivity, and conversion of the raw data to magnetic susceptibility can be found in Refs. [25,26]. The laser beam entered through an ultrahigh vacuum (UHV) window, scattered at 45° from the substrate normal, and exited through a second UHV window. Compensation techniques were used to retain linear polarization after the magneto-optical Kerr rotation. The beam then passed through a polarizing crystal to isolate the rotated component of the light, and was detected by a photodiode. An ac field of 2.0 Oe and 210 Hz was generated by either the in-plane or normal coils, depending upon the experiment, and lock-in detection was used to isolate the signal at the frequency of the field and to measure the susceptibility directly in units of μrad/Oe. Previous studies of this perpendicularly magnetized system [27] have shown that these field parameters produce a linear response in the susceptibility which is sensitive to the slow dynamics of domain walls. The susceptibility was calibrated to dimensionless SI units by using the optical rotation of saturated hysteresis loops of Fe films.

The mutual alignment of the evaporator and MOKE apparatus must be rather precise, and the use of film deposition θ as the independent variable requires growing the films very slowly. To confirm the stability of the mechanical alignment of the evaporator, and the long-term proportionality of deposition time and θ, the following preliminary experiment was performed. Fe/W(110) is known to have an in-plane magnetization with a Curie temperature of 450 K for films 2.0 ML thick [22,28,29]. By using the evaporator calibration found via AES, a film of known Fe thickness near 1.2 ML was grown and annealed at 600 K. Additional deposition
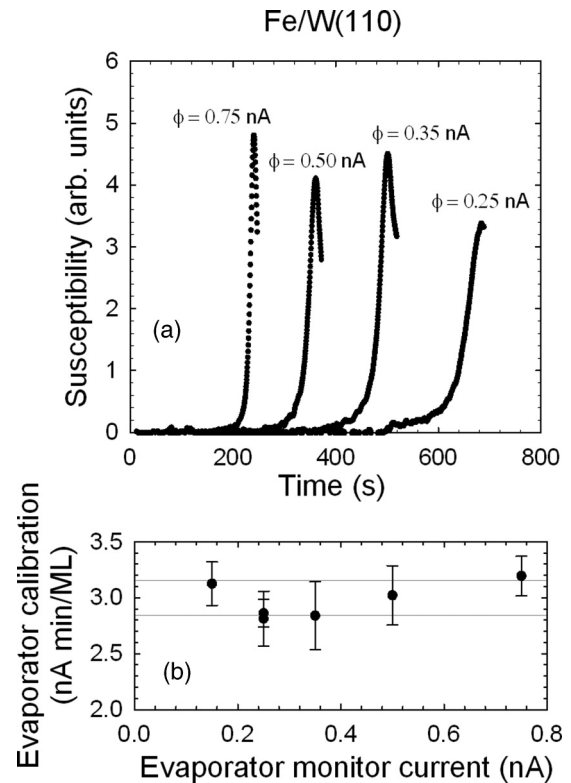

FIG. 1. Proof of principle and growth calibration using Fe/W(110). (a) Starting with Fe films of known thickness near 1.2 ML, the susceptibility is measured as a series of films are grown at 450 K with different evaporator monitor currents in nA. The film undergoes a Curie transition at 2.0 ML. (b) The evaporator is calibrated by using the growth time to the peak in the susceptibility at each monitor current. The band is the error range of the independent calibration using Auger spectroscopy. The error bar on each point reflects the uncertainty in the starting thickness of each film through the Auger thickness calibration.

was then made at a fixed evaporator monitor current ϕ as the susceptibility was measured by using the in-plane coils. This measurement geometry is sensitive to in-plane variations in both the orientation and magnitude of the magnetization via the longitudinal Kerr effect, since it is not affected by demagnetization effects. It is therefore sensitive to an in-plane Curie transition. As is shown in Fig. 1(a), the susceptibility exhibits a narrow peak at the transition from paramagnetism to ferromagnetism as a function of deposition time. Taking the deposition at the peak as 2.0 ML, and knowing the deposition time, an independent calibration of the evaporator was made at each monitor current. These calibration factors are shown in Fig. 1(b). The six calibration points give an average calibration constant of 2.98 ± 0.16 nA min/ML, in agreement with the original AES calibration. This shows that the evaporator is linear and reliably calibrated at low monitor currents, and that the dominant error comes from the Auger calibration method used to determine the thickness of the starting films. With this validation of the experimental procedures, data plots in subsequent sections are presented with ML on the independent axis.

Measurements of the reorientation transition were made in an identical manner, except that the substrate was prepared with 2ML Ni/W(110). The nickel film was annealed to 600 K after deposition of 1 ML to cause wetting of the substrate. In this system [30], the Ni layers create a slightly strained fcc (111) surface template with atomic spacing very close to that of bulk Ni, and in-plane magnetization. Subsequent pseudomorphic Fe deposition creates a system with perpendicular anisotropy. Thicker Fe films reorient to an in-plane magnetization along the [001] in-plane direction of the underlying W(110) crystal [31]. The susceptibility was measured by using a 2.0 Oe ac field normal to the surface. This measurement geometry uses the polar Kerr effect and is sensitive to variations in the orientation of the magnetization normal to the surface and to changes in the net perpendicular magnetization due to domain wall movement [32]. Because the demagnetization factor normal to a thin film is unity, these measurements are not sensitive to changes in the magnitude of the normal magnetization, as might occur, for instance, in a Curie transition for normal magnetization.

III. LONG-RANGE REALIZATION OF SPIN-REORIENTATION TRANSITION

A. Analytic description

A long-range model of the spin-reorientation transition has been used very successfully to describe magnetic susceptibility measurements of perpendicularly magnetized ultrathin films as a function of *temperature* [32]. This has provided information complementary to microscopy studies by describing the dynamics of domain wall formation and pattern defects in the domain pattern [33,34]. In this section, this model is adapted to measurements as a function of thickness.

At a first glance, it is surprising that film thickness can be treated as a continuous variable in ultrathin magnetic films, even though it is a discrete variable with large proportionate changes. This comes about because the exchange interaction is local and (very nearly) uniform, the surface anisotropy $K_S(T)$ is (very nearly) localized to surface and interface layers, and dipole and strain energies are long ranged and effectively average over spatial dimensions. Under these approximations, a basic description of the spin-reorientation transition has no intrinsic scale, and the anisotropy energy E_{an} depends on the surface-to-volume ratio of the film through the temperature and thickness dependence of the effective anisotropy [35], $K_{eff}(T,\theta)$,

$$E_{an} = \sum_i A_i K_S(T) - \sum_i A_i d_i \Omega_D(T), \quad (1)$$

where d_i and A_i are the thickness and surface area of the portions of the film that are i atomic layers thick, and $\Omega_D(T) = \frac{1}{2}\mu_0 M^2(T)$ is the short-range dipolar demagnetization energy for a thin film geometry.

$$K_{eff}(T,\theta) \equiv \frac{E_{an}}{V} = \frac{K_S(T)}{b\theta} - \Omega_D(T), \quad (2)$$

where the total deposition in ML, θ, is given by

$$b\theta = d = \frac{\sum_i A_i d_i}{\sum_i A_i}. \quad (3)$$

b is the thickness of a single atomic layer, and d is the continuous, average thickness. In most cases where a spin-reorientation transition occurs, $K_S(T) > 0$ and the system has magnetization perpendicular to the film at low thickness and/or temperature and a transition to magnetization parallel to the film surface occurs as $K_{eff}(T,\theta)$ changes sign [1] due to an increase in average thickness and/or thermal renormalization of the surface anisotropy with increasing temperature.

At the next level of complexity, the long-range dipole interactions in the perpendicularly magnetized state drive the formation of a domain pattern with equilibrium stripe density [6,10]

$$n^{eq}(T,\theta) = \frac{4}{\pi \ell(T,\theta)} \exp\left(-\frac{E_W(T,\theta)}{4\Omega_D(T)b\theta} - 1\right), \quad (4)$$

where $\ell = \pi[\Gamma/K_{eff}(T,\theta)]^{\frac{1}{2}}$ and $E_W = 4[\Gamma K_{eff}(T,\theta)]^{\frac{1}{2}}$ are the domain wall width and energy per unit area. Γ is the exchange stiffness and the use of the effective anisotropy and average thickness is justified by the long-range nature of the dipole interactions. In the presence of the stripe domain phase, applying a magnetic field along the surface normal causes the domains to grow (shrink) if the domain magnetization is parallel (antiparallel) to the applied field. The equilibrium magnetic susceptibility $\chi_\perp^{eq}(T,\theta)$, measures the moment induced in this way [33]:

$$\chi_\perp^{eq}(T,\theta) = \frac{2}{\pi^2 d}\frac{1}{n^{eq}(T,\theta)} = \frac{\ell}{2\pi b\theta}\exp\left(\frac{E_W(T,\theta)}{4\Omega_D(T)b\theta} + 1\right). \quad (5)$$

The domain walls in the domain pattern are subject to pinning by inhomogeneities in the film, so that the domains respond to the applied field with a relaxation time τ. The relaxation time depends upon the depth, or activation energy E_a, of the local pinning potential and on an intrinsic "attempt" time τ_0 for the trapped domain wall segment to escape:

$$\tau = \tau_0 \exp\left(\frac{E_a}{kT}\right). \quad (6)$$

The pinning sites represent a distribution of activation energies. Bruno *et al.* [36] have considered the question of estimating the mean activation energy due to variations in film thickness. They use a spatial averaging technique to reduce the two-dimensional pinning problem to that of a rigid domain wall moving in a one-dimensional effective potential. Due to the spatial averaging, the resulting mean activation energy depends upon the continuous, average film thickness d:

$$E_a(T,d) = \frac{\zeta d}{E_W(T,d)}\left(\frac{\partial}{\partial d}E_W(T,d)\Delta d\right)^2, \quad (7)$$

where ζ is the mean spacing of pinning sites. Because the pinning is most effective at lower thickness where $K_{eff} \not\approx 0$, $\frac{\Omega_D(T)d}{K_S}$ can be treated as a small parameter in the regime where pinning is effective. Choosing Δd to be a layer thickness b,

$$E_a(T,\theta) \approx \zeta\sqrt{\Gamma K_S(T)b}\,\theta^{-\frac{3}{2}}\left(1 + \frac{3}{2}\frac{\Omega_D(T)b\theta}{K_S(T)}\right). \quad (8)$$

The dynamics of the domain walls in an ac applied field with a low frequency ω can be treated in the relaxation
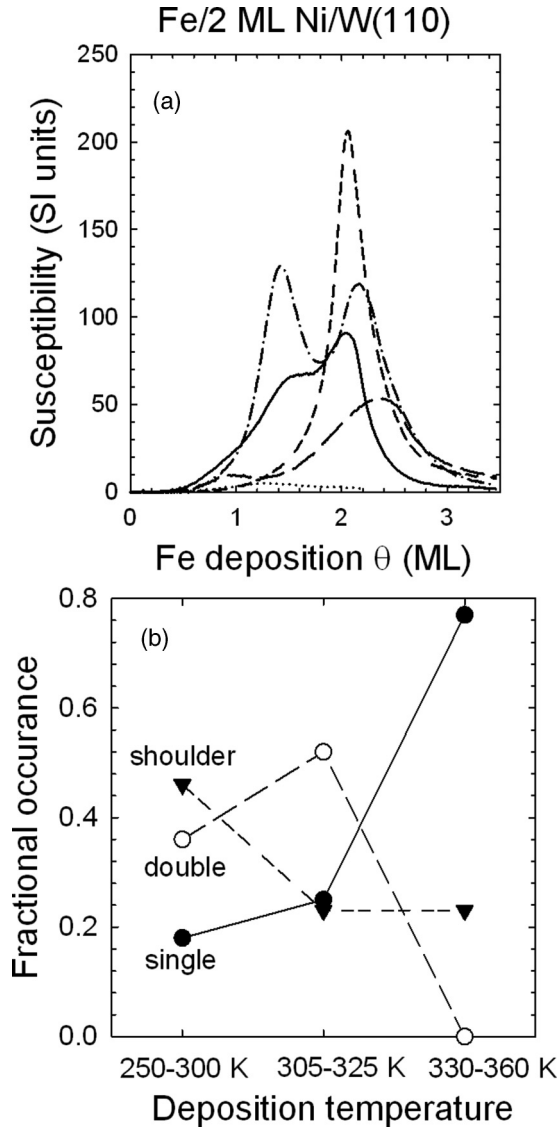
FIG. 2. (a) A selection of susceptibility measurements of Fe/2 ML Ni/W(110) films, measured as a function of coverage as the films were being grown at the following temperatures: 270 K (solid), 315 K (long dash and dash dot), 330 K (short dash). The dotted curve was measured on a film grown at 315 K on a Ni film that was not annealed. These selected curves show the full range of observed qualitative behavior. (b) The frequency with which each type of curve was observed, binned according to the temperature at which the experiment was performed. The peak at lower deposition shows a systematic dependence upon growth temperature.

approximation. This gives

$$\chi_\perp(T,\theta) = \frac{1 - i\omega\tau(T,\theta)}{1 + \omega^2\tau^2(T,\theta)} \, \chi_\perp^{\text{eq}}(T,\theta). \tag{9}$$

In the next section, this model is applied to measurements of the susceptibility as a function of θ.

B. Long-range reorientation as a function of θ

A collection of measurements of $\chi_\perp(\theta)$ for Fe/2 ML Ni/W(110) films is shown in Fig. 2(a). These selected data reflect the full range of qualitative behavior observed in

independent measurements of about 60 different films as they were grown at a variety of constant temperatures from 250 to 360 K. The shape of the curves can be classified qualitatively as (i) a single peak at higher deposition, (ii) a peak at higher deposition with a shoulder at lower coverage, and (iii) two well-resolved peaks. Figure 2(b) shows the frequency with which each category is observed, and how this changes systematically with (binned) temperature.

The peak at high deposition is always observed and occurs just above 2ML of Fe deposition. This is consistent with previous studies [31,37] of the long-range realization of the reorientation transition in films of fixed thickness as a function of temperature. It was possible to measure a susceptibility curve where the peak at high deposition was absent [dotted curve in Fig. 2(a)] by growing on an unannealed Ni film to create a particularly rough Fe film. This is consistent with very strong defect pinning that will not allow domain walls to move at any coverage.

The peak at lower coverage was not anticipated from the earlier studies as a function of temperature. It is more sensitive to the growth conditions, sometimes appearing as a well-resolved peak, and sometimes as a shoulder, with the form depending significantly on the growth temperature. This suggests that the peak at lower deposition is sensitive to the local film microstructure. A successful model for the origin of this peak will account for the systematic dependence of the shape of this peak on growth temperature, as illustrated in Fig. 2(b).

To test these initial interpretations, three measurements taken as films were grown at 315 K, where the two peaks are typically well separated, were selected for quantitative analysis. A sample analysis of the peak at larger θ, using the model for a long-range reorientation transition, is shown in Fig. 3. The fitted curve is mostly obscured by the data points (which have been binned in increments of 0.01 ML). The pinning energies are reduced at high coverage, and the dynamical prefactor in Eq. (9) can be neglected. According to Eq. (5), the logarithm of this portion of the curve should vary as $\theta^{-\frac{3}{2}}$ to first order. This is demonstrated in Fig. 3(b) for the data between the solid arrows. A linear least-squares fit provides the constants $\ln\chi_0$ and C, where

$$C = \frac{\sqrt{\Gamma K_S}}{\Omega_D b^{3/2}}. \tag{10}$$

On the low-coverage side of the peak, the dynamical factor grows as a result of domain wall pinning at lower coverage. This is described by Eqs. (6), (8), and (9). Using the constants from the fit in Fig. 3(b), the scaling of the average activation energy as $\theta^{-\frac{3}{2}}$ is illustrated in Fig. 3(c) for the data between the two dashed arrows. The slope of this plot is given by

$$D = \frac{2\zeta}{k_B T} \sqrt{\Gamma K_S b}. \tag{11}$$

The four constants determined from the two least-squares fits give an excellent description of the peak.

Figure 4 shows that the peak at high deposition in all three of the data sets with well-separated peaks are described very well by the model of the stripe domain pattern that accompanies the long-range realization of the reorientation transition. Microscopy studies showing that the domain
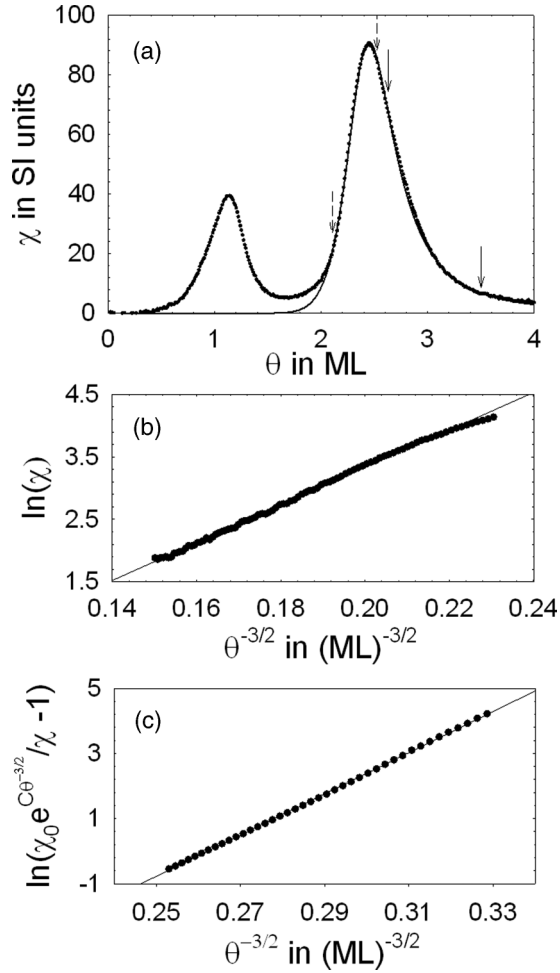
FIG. 3. Representative analysis of the second peak in the susceptibility, using the long-range domain model. (a) Susceptibility of a sample grown at 315 K, with well-separated peaks. The solid line, mostly obscured by the data symbols, is obtained by fitting to the model in Sec. II. (b) The section of the curve in panel (a) between the solid arrows is fit to $\theta^{-\frac{3}{2}}$, in accordance with Eq. (5). (c) The section of the curve in panel (a) between the dashed arrows is fit to $\theta^{-\frac{3}{2}}$, in accordance with Eqs. (6), (8), and (9). The constants χ_0 and C are determined from the fit in panel (b).

density changes exponentially with thickness [14,16,17] are confirmed, with the further finding that the argument of the exponential has a leading term that varies as $\theta^{-3/2}$, as predicted. The data sets with a larger signal in the "valley" between the two peaks likely represent situations where the distribution of pinning activation energies is broader. For this reason, the model based on the mean pinning energy does not fit the tail at low deposition quite as well.

The parameters used to fit the peak at high deposition to the long-range model for reorientation are given in Table I. Using the constants $\Omega_D = 1.86 \times 10^6$ J/m^3 and $\Gamma = 1.49 \times 10^{-11}$ J/m appropriate for bulk iron [38], values for the mean separation of the pinning sites, ζ, and for K_S are calculated and listed in the table. ζ is consistent with a previous study of pinning on Fe/2ML Ni/W(110) films grown near room temperature by using susceptibility measurements as a function of temperature [32], which yielded $\zeta = 58 \pm 9$ nm.
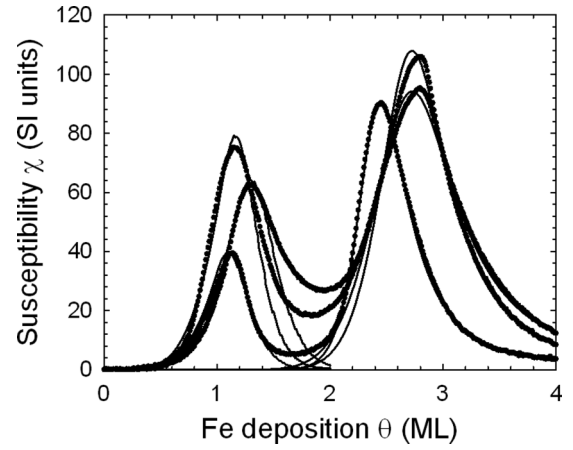

FIG. 4. Selected susceptibility measurements made at 315 K, where the two peaks are well separated. The curves fit to the peaks at higher deposition are based on the model of domain motion in the striped domain pattern that precedes the long-range reorientation transition. The curves fit to the peaks at lower deposition are discussed in Sec. IV.

The values for K_S near room temperature are reasonable, but are about 1.5 times larger than expected. This can be seen from the deposition, θ_R, that these values predict for the reorientation. Table I gives $\theta_R = K_S/(\Omega_D b) \approx 5$ ML, whereas the data in Fig. 4 suggest ≈ 3.5 ML.

A more detailed analysis of the model, including the higher-order terms in Eqs. (5) and (8), is left to a later presentation that considers a larger collection of measurements across a range of temperatures. Nevertheless, it is clear that the model for the long-range realization of the reorientation transition as a function of thickness gives an excellent description of the peak at higher deposition and confirms the identification of this peak. The present article turns now to the new peak at lower deposition.

IV. LOCAL REALIZATION OF REORIENTATION TRANSITION

A. Analytic description

A successful description of the first peak in the susceptibility must be consistent with a number of observations. First, it cannot represent a Curie transition between the paramagnetic and ferromagnetic states of a perpendicularly magnetized film, since demagnetization effects preclude the observation of this

TABLE I. The model for the long-range reorientation mediated by domains yields values for the two dimensionless parameters, C [Eq. (10)] and D [Eq. (11)]. From these, the physical parameters giving the mean separation of pinning sites ζ, the surface anisotropy K_S, and the deposition at which the reorientation transition occurs, θ_R, can be calculated.

Data set	1	2	3
C	30.1 ± 0.2	34.1 ± 0.2	30.0 ± 0.2
D	63.2 ± 0.2	61.4 ± 0.4	50.9 ± 0.3
ζ (nm)	57	49	46
K_S (J/m^2)	1.7×10^{-3}	2.2×10^{-3}	1.7×10^{-3}
$\theta_R = K_S/(\Omega_D b)$ (ML)	4.6	5.9	4.6

type of transition [32]. Second, it cannot involve the motion of domain walls, since these are pinned at all coverages less than the peak at larger θ. The first peak must involve a different low-energy excitation, or "soft" mode, that will respond to a small oscillating perpendicular field. Third, the peak is relatively narrow, occupying a small range of θ near, but significantly above, 1 ML. Finally, the peak is sensitive to the growth conditions, shows systematic changes with the temperature at which the film is grown, and persists even for very rough films.

All these points suggest the magnetic response of islands. There are two possibilities: the peak might be the response of small first-layer Fe islands with perpendicular anisotropy surrounded by the in-plane Ni substrate film, or the peak might represent the response of Fe islands with in-plane anisotropy in the third atomic layer that lie within much larger regions of two-atomic-layer Fe thickness with perpendicular anisotropy. If the first scenario were correct, one would expect the response to begin at much lower coverage than it does, and to reach a maximum well below a coverage of 1 ML. For this reason, the following analytic description is presented with reference to the islands in the third Fe layer. However, the model can be easily adapted to the first scenario, and this question will be revisited.

A number of authors have considered an analytic description of the formation of a static domain wall at the interface between two regions with different axes of magnetic anisotropy [39–41]. Although this description is tractable in one dimension (infinite, uniform stripes), it is much more difficult for two-dimensional islands. A simplified approach that captures the essence of the situation is to assume that there is a critical island radius r_c. Islands in the third layer that have radius $r < r_c$ have a partially developed domain wall at the interface with the two-atomic-layer regions within which they lie. This spin geometry is a compromise between the competing exchange energy with the surrounding two atomic layer region and the in-plane anisotropy energy within the island and represents a system in transition that is sensitive, or "soft", to a small applied perpendicular field. Islands with $r > r_c$ have a fully formed domain wall at their boundary, but the domain wall is pinned and cannot move. In the interior of the islands the in-plane anisotropy and exchange energies are mutually reinforcing, rather than competing, so that there is no significant response to a small perpendicular field.

This simple model is equivalent to determining the net magnetic moment from islands in the third atomic layer below a certain size, and how it responds to an applied perpendicular field. Islands in the third layer grow on larger islands in the second layer, and have in turn islands in the fourth layer growing on top of them. Let s_3 be the number of atoms in a particular island in the third layer of a film, and $N(s_3)$ be the site density of islands in the third layer containing s_3 atoms. The critical island size is when $s_3 = s_3^*$. Then the total site density of islands in the third layer is $N_3 = \sum_{s_3} N(s_3)$. The magnetization that results if the moments of all portions of the film where the surface atoms are in the third layer are aligned is

$$M_{\max} = \left(\frac{1}{a_0^2 3b} \right) \left(\sum_{s_3 < s_3^*} N(s_3) \sum_{s_4 < s_3} \frac{N(s_4)}{N_4} \right) [3\mu(s_3 - s_4)].$$

(12)

The first term is the (site per unit volume). The second is the number of (islands per site), which has been corrected for the fraction of each island in the third layer that is covered by a fourth-layer island. The final term is the (moment per island). a_0 is the in-plane lattice constant, and μ is the moment per atom. The degree to which the spins in the partial domain wall in each island can be aligned by an external perpendicular field H at temperature T is approximately given by multiplying each term under the double sum over s_3 and s_4 in Eq. (12) by the low-field limit of the Langevin function [42]:

$$\frac{1}{3} \left(\frac{3\mu_0 \mu}{kT} (s_3 - s_4) H \right).$$

(13)

Then the susceptibility, in the limit of the applied field going to zero, is

$$\chi_\perp = \frac{2a_0^2 b}{kT} \Omega_D \sum_{s_3 < s^*} N(s_3) \sum_{s_4 < s_3} \frac{N(s_4)}{N_4} (s_3 - s_4)^2,$$

(14)

where it has been recognized that $\frac{1}{2}\mu_0 (\frac{\mu}{a_0^2 b})^2 = \Omega_D$

Amar and Family [43] have presented a model of the island-size distribution as a monolayer film grows. It uses the general scaling condition

$$N(s_i) = \frac{N_i^2}{\theta_i} f(u_i),$$

(15)

where θ_i is the coverage in the ith layer, such that $\theta = \sum_i \theta_i$. $f(u_i)$ is a scaling function in the dimensionless variable $u_i = \frac{s_i}{\sigma_i}$, where σ_i is the average number of atoms contained in each island in the ith layer. An expression for the scaling function is given in Ref. [43]. It has normalization

$$\int_0^\infty f(u)du = \int_0^\infty u f(u)du = 1,$$

(16)

$$\int_0^\infty u^2 f(u)du = 1.09 \equiv c_2.$$

(17)

The function $f(u)$ is such that these integrals are insensitive to the value of the upper limit so long as it is $\geqslant 2$. Substituting these definitions into Eq. (14), and converting the sums to integrals over the continuous variables u_i gives

$$\chi_\perp = \frac{2a_0^2 b}{kT} \Omega_D \int_0^{u_3^*} du_3 N_3 f(u_3) \int_0^{u_4^m} du_4 f(u_4)$$

$$\times \left(\frac{u_3 \theta_3}{N_3} - \frac{u_4 \theta_4}{N_4} \right)^2,$$

(18)

where u_4^m represents the largest island size in the fourth layer, and u_3^* represents the critical island size in the third layer.

It is now assumed that the island growth in the third and fourth layers is beyond the nucleation stage, but still far from layer percolation. Newly deposited atoms are much more likely to aggregate on an existing island than to nucleate a new island. In this aggregation stage [44], the number of islands remains constant. Thus,

$$\sigma_i = \frac{\theta_i}{N_i}.$$

(19)

In addition, since both the third and fourth layers are described by monolayer Fe islands growing on existing Fe islands, the

island density after nucleation has ended will be the same: $N_i = N$. Under these conditions, the upper limits of the integrals can be written as

$$u_3^* = \frac{s_3^*}{\sigma_3} = \frac{s_3^*}{\theta_3} N \equiv \frac{\theta_3^*}{\theta_3}, \tag{20}$$

$$u_4^m = \frac{s_4^m}{\sigma_4} = \frac{s_3}{\theta_4} N = \frac{s_3}{\theta_4} \frac{\theta_3}{\sigma_3} = u_3 \frac{\theta_3}{\theta_4}, \tag{21}$$

and the susceptibility becomes

$$\chi_\perp = B \int_0^{\frac{\theta_3^*}{\theta_3}} du_3 f(u_3) \int_0^{u_3 \frac{\theta_3}{\theta_4}} du_4 f(u_4) (u_3\theta_3 - u_4\theta_4)^2, \tag{22}$$

$$B = \frac{2a_0^2 b}{NkT} \Omega_D. \tag{23}$$

When this expression is used to describe small third-layer islands with radius $r < r_c$, the fourth-layer islands growing on top of them will be very small. Then $u_4^m \sim \frac{\theta_3}{\theta_4} \gg 2$, and the upper limit of the integral over u_4 in Eq. (22) can be replaced by infinity. The final expression for the susceptibility is then

$$\chi_\perp(\theta) = B \int_0^{\frac{\theta_3^*}{\theta_3}} du_3 f(u_3) \left(u_3^2 \theta_3^2 - 2u_3\theta_3\theta_4 + c_2\theta_4^2 \right). \tag{24}$$

To evaluate this requires a model that relates the total deposition θ to the layer coverages θ_i. The most straightforward approach, which is valid at intermediate temperatures, is to assume that newly deposited atoms have sufficient thermal energy to aggregate, but not enough to move from the layer upon which they are deposited to another layer. This condition is described by the differential equation

$$d\theta_i = (\theta_{i-1} - \theta_i) d\theta, \tag{25}$$

which merely states that the ith layer must grow on uncovered regions of the $(i-1)$st layer. It has the solution

$$\theta_i = 1 - e^{-\theta} \sum_{n=0}^{i-1} \frac{\theta^n}{n!}. \tag{26}$$

This can be substituted into each term in Eq. (24) for numerical integration. In the limit of low coverages in the third layer, $\frac{\theta_3^*}{\theta_3} > 2$ and the upper limit of the integral can be set to infinity. Then,

$$\chi_\perp(\theta) = B \left(c_2\theta_3^2 - 2\theta_3\theta_4 + c_2\theta_4^2 \right) \approx B(\theta_3 - \theta_4)^2 = B \frac{\theta^6}{36} e^{-2\theta}. \tag{27}$$

This expression should describe the leading edge of the first susceptibility peak. Recall at this point that it is also conceivable that this peak in the susceptibility represents the response of small islands with perpendicular anisotropy in the first Fe monolayer, which are surrounded by the in-plane Ni substrate. In this case, the leading edge of the peak would vary as

$$\chi_\perp(\theta) \sim (\theta_1 - \theta_2)^2 = \theta^2 e^{-2\theta}. \tag{28}$$
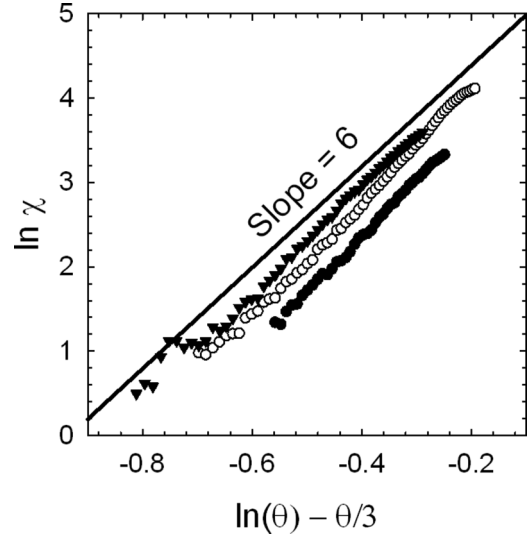

FIG. 5. Scaling of the leading edge of the first peak in the data sets in Fig. 4. According to Eq. (27), the slope should equal 6 if the susceptibility is the response of small islands in the third layer.

B. Local reorientation of islands as a function of θ

The model of local reorientation is tested by applying it to the first peak of the data sets in Fig. 4. In accordance with Eq. (27), the leading edge of the peak with $\theta \leqslant 1 ML$ is plotted in Fig. 5, with $\ln \chi$ as a function of $\ln \theta - \frac{\theta}{3}$.

The fact that the slope on all three of the plots is very nearly 6 is strong evidence that the magnetic response is from small islands of three-layer thickness. It is possible that a peak due to the alternate hypothesis of islands in the first Fe layer will be observable as yet another peak at lower coverage under different experimental conditions. Once the intercept on the plot is used to determine the prefactor B in Eq. (23), the only remaining free parameter is θ_3^*. This is determined by calculating $\chi(\theta)$ in Eq. (24) for a range of values of θ_3^* and finding the value that gives the minimum least-squares deviation from the data. The fitted range of deposition is from zero up to the point where the peak has fallen to twice the susceptibility value in the "valley" between the peaks. Curves fit in this way are included in Fig. 4. The curves give an excellent representation of the data and are for the most part obscured by the data points. Again, in the valley between the two peaks the curves depart significantly from the data. This is likely a result of using a uniform cutoff to the integral, rather than a more nuanced approach that might take into account variables such as island shape, and of course due to overlap with the tail of the second peak.

The fitted values of the parameters B and θ_3^* are collected in Table II. The value of θ_3^* is well within the aggregation regime of the island growth model [44], as was assumed. It can also be used to check the assumption that was made in moving from Eq. (22) to Eq. (24). By rearranging Eq. (21), the condition $u_4^m > 2$ becomes $u_3 > 2\frac{\theta_4}{\theta_3}$. The most stringent test is at the largest value of θ, when $\theta_3 = \theta_3^* \approx 0.2$. In this case, Eq. (26) gives $\frac{\theta_4}{\theta_3} \approx 1/3$, so that $u_3 > 0.67$. This condition omits a portion of the integral in Eq. (22) at small values of u_3. Recalculating the normalization conditions in Eq. (17) from

TABLE II. The model for the local reorientation of islands in the third layer requires the fitting of the two free parameters B and θ_3^*. From these, the physical parameters for the island density N, the critical size s_3^*, and diameter r_c of the islands where there the local transition is complete, can be derived.

Data set	1	2	3
B (SI units)	7670	6190	12 230
θ_3^* (atoms/site)	0.145	0.210	0.165
N/a_0^2 (islands/μm^2)	23	29	15
$a_0^2 s_3^*$ (μm^2/island)	6.2×10^{-3}	7.2×10^{-3}	11.1×10^{-3}
r_c (nm)	45	48	59

this lower limit (rather than 0) shows that a maximum error of 10% is created. This error occurs at the point where the fitted curve is deviating from the data because of the valley between the two peaks in any case. It is concluded that the assumption does not significantly effect the analysis.

The fitted parameters can be related to physical parameters describing the distribution of islands in the third layer. The island density N/a_0^2 can be found from Eq. (23), using the values $\Omega_D = 1.9 \times 10^6$ J/m^3 for bcc iron [38], and $b = 0.20$ nm for the Fe lattice formed on the 2 ML Ni fcc substrate [30]. The critical island area $a_0^2 s_3^*$ can then be found by using Eq. (20), and the radius r_c of the (circular) critical islands calculated. An important point of internal consistency is to compare the calculated critical island radius with the assumptions of the model. According to the model, the magnetic response of the third-layer islands to a small perpendicular field disappears once a complete, pinned domain wall is formed to transition from perpendicular moments at the edge of the island to in-plane moments at the center. Thus the critical island radius should be about the length of a 90° domain wall. The entries in Table II give a average critical island radius of $\approx$50 nm. This is very reasonable for the width of a domain wall.

With the quantitative success of the local model of the spin-reorientation transition for measurements taken at 315 K, it can be applied to the interpretation of the systematic variation in the shape of the first peak with temperature, as seen in Fig. 2(b). A key assumption of the model is that the mobility of the deposited Fe atoms is large enough to allow the aggregation of atoms onto existing islands once the fitted island density has been nucleated. A second assumption, implied by Eq. (25), is that the mobility of the Fe atoms is not large enough to allow them to move between atomic layers. This suggests that there is a restricted range of mobilities where both assumptions can be correct, and two well-separated peaks in the susceptibility can be observed. According to Fig. 2(b), this mobility evidently occurs in the temperature range 305–325 K, where the measured susceptibility most commonly has a double-peak structure.

At higher temperature (330–360 K), the mobility is increased and the occurrence of a susceptibility with a single peak at high deposition increases markedly at the expense of occurrences of a double-peak structure. The implication is that the increased mobility now permits Fe atoms to move from one layer to another, so that when $\theta \approx 1 ML$ they do not aggregate

on the third-atomic-layer islands, but rather move to vacancies in the second layer to form a more perfect film. Since this will greatly reduce the island density in the third layer and increase the size of the remaining islands, the susceptibility due to third-layer islands within the critical size will be greatly reduced.

At lower temperature (250–300 K), the mobility is decreased, and the occurrence of a susceptibility with a small shoulder increases at the expense of occurrences of a double peak structure. The implication is that the decreased mobility no longer permits the same degree of aggregation of atoms on the third-layer islands, so that the island density increases and the islands are much smaller on average. This results in only a shoulder, or a small peak at lower deposition. Thus the identification of the newly observed peak in the susceptibility as a local realization of the reorientation transition is supported not only by the quantitative description of data curves in the intermediate temperature range where both peaks are well-resolved, but also by the qualitative explanation of the systematic changes in this peak as a function of temperature that it provides.

V. CONCLUSIONS

Novel *in situ* measurements of the magnetic susceptibility of Fe/2 ML Ni/W(110) films, made as a function of deposition as the films were grown, have provided a more comprehensive view of the collection of related phenomena that are referred to as the surface spin-reorientation transition. The measurements reveal two clear peaks in the susceptibility associated with the transition, rather than the single peak that might have been inferred from microscopy studies or studies as a function of temperature. The peak at lower coverage is sensitive to details of the film growth and, although its precise form is not precisely reproducible from film to film, it shows systematic changes with the temperature at which the experiment is performed. In an intermediate temperature range near 315 K, the two peaks are commonly well separated so that they can be modelled and analyzed separately.

The peak at larger deposition ($\theta \geqslant 2$ Fe ML) results from the long-range realization of the reorientation transition, where the energetics are governed by mesoscopic averaging over the film morphology and lead to long-range domain structures. This signature peak is well described by an analysis in terms of the continuous average film thickness, or total deposition, θ. The peak is a response to the motion of domain walls in the stripe domain pattern. The domain density is found to be an exponential function of average film thickness, in agreement with previous microscopy studies. It is further shown that the functional form of the argument of the exponential has a leading term that varies as $\theta^{-3/2}$, in agreement with theory. The domain walls are pinned with an activation energy that also varies as $\theta^{-3/2}$, but through a different mechanism. This variation results from the mean of the distribution of the averaged effective pinning potential due to statistical variations in film thickness. The model gives an excellent description of the magnetic susceptibility with only four independent parameters. A more extensive investigation of the long-range thickness-dependent transition will be the subject of a future presentation.

The peak at lower deposition ($\theta \leqslant 1.5$ Fe ML) is described quantitatively by a local realization of the reorientation transition, where the effects of finite size and metastability are important. As a result, the reorientation must be described in terms of local, discrete layer thickness and coverages θ_i rather than the total deposition. The discrete step in thickness between the second and third layers creates a boundary between regions with perpendicular and in-plane anisotropy. The partial domain wall pinned at this boundary on islands smaller than a critical radius is susceptible to a small perpendicular field. The model of the response of the islands in a local realization of the transition has only two free parameters. First, the leading edge of the susceptibility peak scales as $\chi_\perp(\theta) \sim \theta^6 \exp(-2\theta)$, in agreement with the aggregation of small third-layer islands on the second layer. Second, the response disappears once the third-layer islands have a radius larger than ≈ 50 nm, which is

a consistent with the formation of a complete pinned domain wall at the island boundary.

These results make it clear that both the local and long-range realizations of the reorientation transition are needed to understand the magnetic response of the system. The two realizations are distinct in that they involve different magnetic excitations, different descriptions of the film morphology, and occur at different locations in parameter space. They are tied together within the group of related phenomena that result from the rebalancing of dipole energy and anisotropy energy as the temperature and/or average thickness of an ultrathin film is varied.

[1] Y. Millev and J. Kirschner, Phys. Rev. B **54**, 4137 (1996).

[2] C. S. Arnold, D. P. Pappas, and A. P. Popov, Phys. Rev. Lett. **83**, 3305 (1999).

[3] J. P. Pierce, M. A. Torija, J. Shen, and E. W. Plummer, Phys. Rev. B **64**, 224409 (2001).

[4] Many examples are in *Ultrathin Magnetic Structures*, edited by J. A. C. Bland and B. Heinrich (Springer, 1994), Vol. 1, Sec. 2.3.

[5] R. Allenspach and A. Bischof, Phys. Rev. Lett. **69**, 3385 (1992).

[6] A. B. Kashuba and V. L. Pokrovsky, Phys. Rev. B **48**, 10335 (1993).

[7] K. De'Bell, A. B. MacIsaac, and J. P. Whitehead, Rev. Mod. Phys. **72**, 225 (2000).

[8] O. Portman, A. Vaterlalus, and D. Pescia, Nature (London) **422**, 701 (2003).

[9] M. Kronseder, T. N. G. Maier, M. Zimmermann, M. Buscher, M. Vogel, and C. H. Back, Nat. Commun. **6**, 6832 (2015).

[10] A. Abanov, V. Kalatsky, V. L. Pokrovsky, and W. M. Saslow, Phys. Rev. B **51**, 1023 (1995).

[11] A. Vaterlaus, C. Stamm, U. Maier, M. G. Pini, P. Politi, and D. Pescia, Phys. Rev. Lett. **84**, 2247 (2000).

[12] S. A. Cannas, M. F. Michelon, D. A. Stariolo, and F. A. Tamarit, Phys. Rev. B **73**, 184425 (2006).

[13] N. Bergeard, J. P. Jamet, A. Mougin, J. Ferré, J. Gierak, E. Bourhis, and R. Stamps, Phys. Rev. B **86**, 094431 (2012).

[14] C. Won, Y. Z. Wu, J. Choi, W. Kim, A. Scholl, A. Doran, T. Owens, J. Wu, X. F. Jin, H. W. Zhao, and Z. Q. Qui, Phys. Rev. B **71**, 224429 (2005).

[15] M. Kronseder, M. Bucher, H. G. Bauer, and C. H. Back, Nat. Commun. **4**, 2054 (2013).

[16] M. Dabrowski, M. Cinal, M. Przybylski, G. Chen, A. T. N'Diaye, A. K. Schmid, and J. Kirschner, Phys. Rev. B **93**, 064414 (2016).

[17] R. Zdyb and E. Bauer, Phys. Rev. B **67**, 134420 (2003).

[18] A. Kubetzka, O. Pietzsch, M. Bode, and R. Wiesendanger, Phys. Rev. B **63**, 140407 (2001).

[19] F. El Gabaly, S. Gallego, C. Muñoz, L. Szunyogh, P. Weinberger, C. Klein, A. K. Schmid, K. F. McCarty, and J. de la Figuera, Phys. Rev. Lett. **96**, 147202 (2006).

[20] D. Venus, Rev. Sci. Instrum. **62**, 1361 (1991).

[21] T. Jones, J. Sawler, and D. Venus, Rev. Sci. Instrum. **64**, 2008 (1993); T. Jones and D. Venus, Surf. Sci. **302**, 126 (1994).

[22] Examples can be seen in K. Fritsch, R. D'Ortenzio, and D. Venus, Phys. Rev. B **83**, 075421 (2011).

[23] A. Berger, S. Knappmann, and H. P. Oepen, J. Appl. Phys. **75**, 5598 (1994).

[24] C. H. Back, C. Würsch, A. Vaterlaus, U. Maier, and D. Pescia, Nature (London) **378**, 597 (1995).

[25] C. S. Arnold, M. Dunlavy, and D. Venus, Rev. Sci. Instrum. **68**, 4212 (1997).

[26] C. S. Arnold and D. Venus, Rev. Sci. Instrum. **66**, 3280 (1995).

[27] D. Venus and M. J. Dunlavy, J. Magn. Magn. Mater. **260**, 195 (2003).

[28] H. J. Elmers, J. Hauschild, H. Fritzsche, G. Liu, U. Gradmann, and U. Köhler, Phys. Rev. Lett. **75**, 2031 (1995).

[29] M. J. Dunlavy and D. Venus, Phys. Rev. B **69**, 094411 (2004).

[30] H. L. Johnston, C. S. Arnold, and D. Venus, Phys. Rev. B **55**, 13221 (1997).

[31] C. S.Arnold, H. L. Johnston, and D. Venus, Phys. Rev. B **56**, 8169 (1997).

[32] D. Venus, C. S. Arnold, and M. Dunlavy, Phys. Rev. B **60**, 9607 (1999).

[33] N. Abu-Libdeh and D. Venus, Phys. Rev. B **84**, 094428 (2011).

[34] N. Abu-Libdeh and D. Venus, Phys. Rev. B **81**, 195416 (2010).

[35] B. Heinrich and J. F. Cochran, Adv. Phys. **42**, 523 (1993).

[36] P. Bruno, G. Bayreuther, P. Beauvillain, C. Chappert, G. Lugert, D. Renard, J. P. Renard, and J. Seiden, J. Appl. Phys. **68**, 5759 (1990).

[37] M. J. Dunlavy and D. Venus, Phys. Rev. B **62**, 5786 (2000).

[38] S. Chikazumi, *Physics of Magnetism*, 2nd ed. (Clarendon Press, 1997), p. 415 and Appendix 4, respectively.

[39] H. J. Elmers, J. Magn. Magn. Mater. **185**, 274 (1998).

[40] H. J. Elmers, J. Hauschild, and U. Gradmann, Phys. Rev. B **59**, 3688 (1999).

[41] N. Weber, K. Wagner, H. J. Elmers, J. Hauschild, and U. Gradmann, Phys. Rev. B **55**, 14121 (1997).

[42] Reference [38], Sec. 5.2.

[43] J. G. Amar and F. Family, Phys. Rev. Lett. **74**, 2066 (1995).

[44] J. G. Amar, F. Family, and P.-M. Lam, Phys. Rev. B **50**, 8781 (1994).